Mechanisms of Tubulogenesis and Endothelial Phenotype Expression by MSCs

Julie A Rytlewski[1,2], **M Alejandra Aldon**[1], **Evan W Lewis**[1], and **Laura J Suggs**[1]

Julie A Rytlewski: julie.rytlewski@utexas.edu; M Alejandra Aldon: alejandra.aldon@utexas.edu; Evan W Lewis: evan.lewis@utexas.edu

[1]Department of Biomedical Engineering, The University of Texas at Austin, 107 W Dean Keeton, Stop C0800, Austin, Texas 78712 USA

Abstract

Stem cell-based therapies are a promising new avenue for treating ischemic disease and chronic wounds. Mesenchymal stem cells (MSCs) have a proven ability to augment the neovascularization processes necessary for wound healing and are widely popular as an autologous source of progenitor cells. Our lab has previously reported on PEGylated fibrin as a unique hydrogel that promotes spontaneous tubulogenesis of encapsulated MSCs without exogenous factors. However, the mechanisms underlying this process have remained unknown. To better understand the therapeutic value of PEGylated fibrin delivery of MSCs, we sought to clarify the relationship between biomaterial properties and cell behavior. Here we find that fibrin PEGylation does not dramatically alter the macroscopic mechanical properties of the fibrin-based matrix (less than 10% difference). It does, however, dramatically reduce the rate of diffusion through the gel matrix. PEGylated fibrin enhances the tubulogenic growth of encapsulated MSCs demonstrating fluid-filled lumens by interconnected MSCs. Image analysis gave a value of 4320±1770μm total network length versus 618±443μm for unmodified fibrin. PEGylation promotes the endothelial phenotype of encapsulated MSCs—compared to unmodified fibrin—as evidenced by higher levels of endothelial markers (von Willebrand factor, 2.2-fold; vascular endothelial cadherin, 1.8-fold) and vascular endothelial growth factor (VEGF, up to 1.8-fold). Prospective analysis of underlying molecular pathways demonstrated that this endothelial-like MSC behavior is sensitively

Corresponding Author. Laura J Suggs, 107 W Dean Keeton, Stop C0800, Austin, Texas 78712 USA, laura.suggs@engr.utexas.edu, tel: +1 512-232-1671, fax: +1 512-471-0616.
[2]Present address: Division of Human Biology, Fred Hutchinson Cancer Research Center, 1100 Fairview Avenue N, D4-100, Seattle, Washington 98109 USA

modulated by hypoxic stress, but not VEGF supplementation as evidenced by a significant increase in VEGF and MMP-2 secretion per cell under hypoxia. Further gain-of-function studies under hypoxic stress demonstrated that hypoxia culture of MSCs in unmodified fibrin could increase both vWF and VE-cadherin levels to values that were not significantly different than cells cultured in PEGylated fibrin. This result corroborated our hypothesis that the diffusion-limited environment of PEGylated fibrin is augmenting endothelial differentiation cues provided by unmodified fibrin. However, MSC networks lack platelet endothelial cell adhesion molecule-1 (PECAM-1) expression, which indicates incomplete differentiation towards an endothelial cell type. Collectively, the data here supports a revised understanding of MSC-derived neovascularization that contextualizes their behavior and utility as a hybrid endothelial-stromal cell type, with mixed characteristics of both populations.

INTRODUCTION

Autologous cell-based therapies are a developing strategy to address ischemic morbidities and promote perfusion of oxygen- and nutrient-deprived tissue. Currently, common targets include sites of acute injury, large or chronic wound beds, and critical limb ischemia (Fadini et al., 2010). For these applications, the end-goal is to achieve revascularization, which is often the rate-limiting step in wound healing (Gibot et al., 2010). Establishing a robust blood supply better sustains the high metabolic demands of inflammation and tissue remodeling and promotes more rapid resolution of the damaged tissue (Gibot et al., 2010). Healing outcomes have been further improved when biomaterial gels, foams, or scaffolds are co-delivered with the grafted stem cells (Kim et al., 2011). These biomaterials serve a threefold purpose: (1) to act as a cell delivery vehicle, (2) to enhance and direct stem cell behavior, and (3) to serve as bioactive filler that physically and biochemically integrates with local tissues.

Our group has previously reported on PEGylated fibrin as a natural-synthetic polymer composite that promotes tubulogenesis of encapsulated bone marrow-derived mesenchymal stem cells (MSCs), without added soluble factors (Zhang et al., 2010). Here, PEGylation slows fibrinolysis and extends the therapeutic window of MSCs localized within the matrix. Additionally, bone marrow-derived MSCs serve as a readily available autologous progenitor population that are responsive to substrate cues (Lutolf et al., 2009) and have a proven history of enhancing angiogenic activity and wound closure (Falanga et al., 2007). While we have previously observed a dramatic increase in tubulogenic development of MSCs in PEGylated fibrin gels (compared to fibrin) (Rytlewski et al., 2012), the full breadth of differences in cellular behavior has not yet been characterized, nor have the underlying mechanisms. Understanding how PEGylation changes biomaterial properties is critical to understanding why MSC network development is significantly improved. Furthermore,

gaining a clearer understanding of this cell-gel system will facilitate a more targeted context for its potential clinical implementation.

The series of *in vitro* studies presented here aims to characterize the biophysical properties of PEGylated fibrin gels and subsequent cell behavior associated with neovascularization events: lumenal space formation, production of matrix remodeling and paracrine factors, and markers of an endothelial phenotype. Possible matrix cues were then isolated to determine which cues yielded specific neovascularization events.

METHODS

Materials

Low-glucose Dulbecco's modified Eagle's medium (DMEM), phosphate buffered saline (PBS), fetal bovine serum (FBS), and Gluta-MAX™-I (100×) were purchased from Invitrogen (Carlsbad, CA). Penicillin-streptomycin and trypsin/ethylenediaminetetra-acetic acid were purchased from ATCC (Manassas, VA). Sigma-Solohill microcarrier beads (MCBs) coated in porcine collagen were obtained from Sigma-Aldrich (St. Louis, MO) as well as fibrinogen and thrombin from human plasma. Linear homo-difunctional polyethylene glycol succinimidylglutarate (PEG-$(SG)_2$, 3400 Da) was purchased from NOF America (White Plains, NY).

PEGylated fibrin gel fabrication

Gel fabrication followed our previously described protocol for enzymatically crosslinked PEGylated fibrin and fibrin gels (Rytlewski et al., 2012; Zhang et al., 2010). Human fibrinogen was solubilized in PBS (without calcium or magnesium, pH 7.8) at 8× the desired final concentration. PEG-SG_2 was similarly dissolved in PBS. Human thrombin was reconstituted in nanopure ddH_2O to 100U/mL and diluted to 25U/mL with 40mM $CaCl_2$. Gel components were sterilized with 0.22μm syringe filters. Gel components were mixed in the following order (volume ratio): (1) fibrinogen, (1) PEG-SG_2, (2) PBS for rheology or MSC-seeded MCBs for cell studies (4) thrombin. Gelation was finalized at 37°C for 15min before rinsing with PBS (with calcium and magnesium).

Rheology

Gels were prepared without cells in 40mm diameter nonstick molds for a parallel plate rheometer configuration and were kept hydrated with PBS prior to and during testing. Strain sweeps were measured from 0.1–2.5% at 15 rad/s at a plate temperature of 37°C. Storage and loss moduli were reported for statistical comparison at 1% strain.

Cryogenic scanning electron microscopy

Cell-free gels were prepared in small-volume molds and kept hydrated in PBS (with calcium and magnesium). Gels were briefly rinsed in ddH_2O before mounting on a cryogenic SEM stage with carbon tape. Mounted gels were then snap-frozen in liquid nitrogen and fractured with a scalpel to expose cross-sectional structures. Gels were transferred to the cryo prep unit within a vacuum cryo transfer shuttle (Leica EM VCT100) to minimize crystal formation from air exposure. In the prep unit (Leica EM MED020), the stage temperature

was raised from –140°C to –110°C to sublimate water crystals from the gels. Samples were then sputter coated with palladium and shuttle-transferred to the SEM for imaging. The SEM stage was kept at –120°C to –123°C for the duration of imaging.

Diffusional characterization

Syringes (without the plunger) were used as molds for containing fibrin or PEGylated fibrin gels and the test solute. Cell-free gels (500μL volume) were formed at the 0cc demarcation of the syringe barrel, gelled to completion at 37°C, and rinsed with an equal volume of PBS. After the PBS was aspirated, the slip-tips of the syringes were carefully removed to expose the gel bottoms. Removal of the slip-tips ensured that diffusivity of the test solute was limited by the gel and not by capillary resistance of the solvent through the syringe. Syringes were vertically fixed in place and 500μL of 2.5mg/mL 10kDa dextran-Texas Red conjugate (Molecular Probes; Eugene, OR) was added directly on top of the gels. While fluorescence was not utilized, the purple appearance of Texas Red dye provided clear visualization of the dextran. Time-lapse photos of dye diffusion were taken every 15min for 7h.

Expansion and Maintenance of Cells

Human bone marrow-derived mesenchymal stem cells (MSCs; Lonza; Basel, Switzerland) were cultured according to manufacturer specifications with growth medium in tissue culture-treated plastic flasks at 5000 cells/cm^2. Growth medium consisted of DMEM supplemented with 10% FBS, 1% penicillin-streptomycin, and 2mM GlutaMAX™-I. MSCs were tested by the manufacturer for trilineage differentiation potential and for positive expression of CD105, CD166, CD29, and CD44; cells were negative for CD14, CD34, and CD45. Population purity was greater than 95%.

For gel cultures, cells were seeded on MCBs according to our previously described protocol, based on the modified bead-outgrowth assay developed by Nakatsu and Hughes (Nakatsu et al., 2007; Nakatsu and Hughes, 2008; Nehls and Drenckhahn, 1995). Briefly, cells at passages 4–6 were trypsinized, centrifuged into a pellet, and re-suspended in media at a minimum concentration of 1.4×10^5 cells/mL. MSCs were seeded at 7.0×10^4 cells/mg MCB. Cells and MCBs were gently agitated every 30min over 4h and then transferred to ultra-low adhesion 6-well plates for further coating overnight. Cell-seeded MCBs were strained through a 70μm mesh and resuspended in 300μL growth media/mg MCB prior to encapsulation in gels. Gels were thoroughly rinsed with growth media to remove cytotoxic unreacted PEG-SG$_2$. Gel culture was carried out to Day 7 with growth media unless otherwise specified.

Small molecules for functional assays

For some experimental groups, small molecules, proteins, or peptides were added to culture media. Table 1 lists each molecule, the concentration used, the experimental study in which it was applied, and the manufacturer's information.

Hypoxic cell culture

Where indicated, MSCs were also cultured under 1% O$_2$ and 2% O$_2$ using a hypoxia chamber (Stemcell Technologies; Tukwila, WA), generously loaned to us by Dr. Aaron

Baker. Hypoxic gas mixes were composed of 5% CO_2, 1% or 2% O_2, and N_2 balance (Praxair; Danbury, CT). Cell cultures were environmentally isolated inside the hypoxia chamber with an open petri dish of water for humidity and kept at 37°C. The chamber was purged with hypoxic gas for 5min and then purged again 90min later to evacuate any residual oxygen. Thereafter, the chamber was purged every 48h to maintain hypoxic cultures unless opened for assay endpoints.

Fluorescent cell staining for visualizing vacuolar compartments

Texas Red-conjugated dextran (10kDa; Molecular Probes; Eugene, OR) was added to the media of gel cultures as a cell-impermeable dye for pinocytic uptake (Davis and Camarillo, 1996). For Day 7 endpoint cultures, 1.25mg/mL of dextran was added on Day 4; for Day 10 endpoint cultures, dextran was added on Day 7. After cultures were terminated, MSCs were fixed and additionally stained with FITC-phalloidin (F-actin) and DAPI (nuclei).

Fluorescent cell staining for morphological quantification

On day 7 of gel culture, samples were thoroughly rinsed with PBS (with calcium and magnesium) for 1h. Calcein AM (Invitrogen; Carlsbad, CA) was added at 10μM for 1h to stain the cytoplasm of live cells. Samples were again rinsed with PBS and then fixed with 4% neutral-buffered formalin for 30min. Samples underwent a final PBS rinse and stored at 4°C overnight for imaging the next day.

Two-photon microscopy

Fluorescent z-stacks were collected of MSC outgrowth from individual microcarrier beads with an Ultima Multiphoton Microscopy System (Prairie Technologies; Middleton, WI). Simultaneous two-photon excitation of multiple fluorophores was achieved with was achieved with a tunable Ti:sapphire laser (Spectra-Physics Mai Tai HP; Newport; Irvine, CA) set to 720nm. Z-slice thickness was adjusted to maintain isometric voxel dimensions. A thickness of 500–700μm was imaged along the z-axis for each image stack.

Three-dimensional morphological quantification

Image processing and three-dimensional morphological quantification followed our recently described method (Rytlewski et al., 2012). As before, z-stacks were preprocessed in ImageJ (Release 1.2.4; ImageJ Plugin Project) and loaded into 3D Slicer (Release 3.6, 64-bit Linux). The Vascular Modeling Toolkit in 3D Slicer was used for image segmentation and 3D model generation. Centerline tracings of 3D models were exported as large data clouds of x,y,z coordinates with corresponding model radii. The data cloud was processed in MATLAB (Release 2008a for Macintosh) to calculate the average 3D network length per MCB.

Cell proliferation

The CellTiter 96® Aqueous One Solution Cell Proliferation Assay (Promega; Madison, WI) was used to quantify the cell content of gels. On days 1, 3, 5, and 7 of gel culture, the culture supernatant was removed and saved for secreted protein analysis. Fresh growth media + 20% (v/v) CellTiter 96® solution was then added for 4h. Supernatants were transferred in

triplicate to a 96-well plate. Absorbance was measured at 490nm with a microplate reader (BioTek Synergy HT Multi-Mode Microplate Reader; Winooski, VT).

Secreted protein detection by ELISA

Quantikine ELISA kits (R&D Systems; Minneapolis, MN) were procured for VEGF, matrix metalloproteinase-2 (MMP-2), and MMP-9. Supernatant collected from cell proliferation samples were assayed according to the manufacturer's instructions. Optical density was measured at 490nm. Secreted protein quantities were normalized to cell number using the results of the matched-sample MTS assay.

Cellular protein detection by western blot

Cells in gels were lysed with RIPA buffer (Santa Cruz Biotechnology; Dallas, TX) and homogenized with a soft tissue grinder (OMNI International; Kennesaw, GA). Cell-gel lysates were passed through a 21-gauge needle 20× for further homogenization and solid gel remnants were removed through centrifugation. Supernatants were denatured in Laemmli buffer with 5% β-mercaptoethanol at 95°C for 5min. Denatured samples were separated with 10% mini-Protean® TGX™ precast gels (Biorad; Hercules, CA) at 20μg protein per gel lane and blotted onto PVDF membranes. Membranes were blocked for 1h at room temperature with 5% (w/v) nonfat milk in TBST and then incubated overnight with a primary antibody at 4°C. Membranes were rinsed with TBST and incubated with an HRP-conjugated secondary antibody for 1h at room temperature. After a second set of TBST rinses, 3mL of SuperSignal West Dura Chemiluminescent Substrate (Pierce Thermo Fisher Scientific; Rockford, IL) was added per membrane for 5min prior to image capture with a FluorChem CCD system (ProteinSimple; Santa Clara, CA). Chemiluminescent signal was quantified with AlphaView software for statistical analysis. For a list of antibodies and their dilutions, refer to Table 2.

Statistical analysis

A one- or two-way analysis of variance was used to determine significance between experimental groups. Where significance was found, post-hoc tests were performed to further determine specific relationships of statistical significance. Tukey's correction for multiple comparisons was applied where appropriate. P-values less than 0.05 were considered statistically significant. All statistical tests were completed in Prism (Version 6.0 for Mac OS X; GraphPad, La Jolla, CA).

RESULTS

Macro- and microscopic changes associated with fibrin PEGylation

Rheological characterization of PEGylated fibrin gels in Figure 1A showed little change in their viscoelastic properties over unmodified fibrin gels when matched by fibrin concentration. At 10mg/mL, fibrin gels (10F) had a statistically significant increase in their elastic modulus over PEGylated fibrin (10P) but the magnitude of this increase was less than 10% of the storage modulus. Both PEGylated fibrin and fibrin gels demonstrated increasing elastic moduli with increasing fibrin concentration, corresponding to the crosslinking density of the matrix (approximately 50Pa, 75Pa and 125Pa for 5mg/mL, 7.5mg/mL and 10mg/mL 10P, respectively). Despite similar mechanical properties, cryo-SEM (Figure 1B–E)

revealed remarkable differences in the fibrin gel microstructure introduced by PEGylation. Unmodified fibrin (10F) had a stereotypical fibrous and sponge-like appearance. PEGylated fibrin (10P), in contrast, had non-porous amorphous layers interspersed within the fibrous architecture. This amorphous quality is associated with a significant change in fibrin's diffusional characteristics. In Figure 1F, time-lapse photography of labeled 10kDa dextran showed both slowed diffusion of the dextran solute and slower filtration of the PBS solvent through PEGylated fibrin (10P) over unmodified fibrin (10F) gels.

MSC in PEGylated fibrin form hollow tubes with endothelial markers

We have previously reported that networks formed by MSCs in PEGylated fibrin were significantly longer than those encouraged by fibrin alone (Rytlewski et al., 2012), indicating that PEGylated fibrin is superior in promoting tubulogenesis. Here, we further characterize important neovascular features of MSC networks and seek to correlate these features with the material properties of PEGylated fibrin matrices. The presence of intra- and inter-cellular vacuolar compartments is the first step in lumen formation and was the first key characteristic we examined. Based on a lumenization study by George Davis's group on endothelial network development (Davis and Camarillo, 1996), gel culture media was doped with membrane-impermeable 10kDa dextran-Texas Red. Pinocytosed vesicles (containing the labeled dextran) are known to fuse with vacuolar compartments (K. Bayless and Davis, 2002). Hence, these lumenal spaces, if present, can be visualized by the intracellular localization of the fluorescent dextran. Fluorescent microscopy of MSC networks in PEGylated fibrin (10P) showed large intracellular compartments of fluorescent dextran that spanned multiple cell lengths (Figure 2A–C), suggesting intercellular vacuole fusion had occurred. These large vacuolar spaces with non-overlapping nuclei and narrow tube diameter are highly reflective of cell-hollowing lumen assembly associated with small capillary development (Lubarsky and Krasnow, 2003). In contrast, lower magnification views of cells in fibrin gels (10F, Figure 2D) do not demonstrate interconnected networks relative to similar views of cells in PEGylated fibrin, (10P, Figure 2E).

Mediators of MSC motility in PEGylated fibrin (10P) during tubulogenesis and lumenization were identified by examining components of the matrix-integrin-cytoskeletal (MIC) axis (Davis et al., 2002). As in normal endothelial network development, MSCs exhibited a strong dependence on microtubule assembly and integrin-mediated binding. In Figure 3B–D & G, colchicine (a tubulin inhibitor) caused a more dramatic decrease in network assembly than cytochalasin B (an actin inhibitor), although both were statistically significant. Additionally, cyclic-RGD inhibition of cell motility (Figure 3E–G) effectively eliminated network outgrowth, while control peptides of cyclic-RGE were not statistically different from controls. This result implicates αvβ3 and α5β1 as likely integrins responsible for MSC adhesion to PEGylated fibrin and is consistent with current literature regarding how endothelial cells interact with fibrin-based matrices.

Secreted and cellular proteins were analyzed to provide evidence of endothelial-like MSC behavior. Total protein secretion of VEGF and MMP-2 was higher in fibrin gels than in PEGylated fibrin (not shown). However, the metabolic assay indicated a slower growth rate of MSCs in PEGylated fibrin (10P, Figure 3H). When protein production was normalized to

cell number, we found that MSCs in PEGylated fibrin (10P) secreted significantly larger quantities of early (days 1 and 3) VEGF and late (days 3, 5 and 7) MMP-2 than MSCs in fibrin alone (10F, Figure 3I & J). Western blot of cellular proteins showed that MSCs in both matrices (Fibrin and PEGylated fibrin) under normoxia also expressed vWF and VE-cadherin proteins (Figure 5I), which are considered highly specific to endothelial populations (Pusztaszeri et al., 2006). Interestingly, PECAM-1 protein expression was not detected from either matrix (Supplemental Material Figure 1).

Hypoxia activation is more important to MSC proliferation and secretion than direct VEGF stimulation

Potential stimuli from the microenvironment were tested to pinpoint the key pathway responsible for catalyzing MSC transformation towards an endothelial-like cell type. The sensitivity of MSC tubulogenesis in PEGylated fibrin to chemically simulated hypoxia (CoCl$_2$) (Piret et al., 2002), true hypoxia (1% O$_2$), and soluble VEGF (Figure 4A–D) was assessed by quantification of network development, cell proliferation, and angiogenic protein production.

Induction of cellular hypoxia with 1% O$_2$ was confirmed by ELISA for HIF-1α protein (Figure 4E); protein was normalized to DNA content of the sample to account for different cell proliferation rates under normoxic and hypoxic conditions. Significant upregulation was demonstrated under 1% hypoxia in PEGylated fibrin (10P) versus normoxia. As diagrammed in Figure 4F, upregulation of HIF-1α is specifically known to stimulate neovascularization processes. Quantification of MSC network lengths (Figure 4G) indicated that VEGF, CoCl$_2$, and 1% O$_2$ all resulted in shorter networks than the control group (10P), though 1% O$_2$ was not statistically significant. Growth rate quantification, however, revealed that 1% O$_2$ significantly reduced the number of MSCs cultured in 10P from Day 3 onward (Figure 4H). When secreted VEGF and MMP-2 were again analyzed, we found that only 1% O$_2$ significantly increased the production of both proteins over the control normoxic group (Figure 4I & J). Others have similarly reported a lack of MSC sensitivity to soluble VEGF and emphasized the importance of other variables, such as cell density, over supplemental growth factors (Galas and Liu, 2013). From this study, we concluded that MSCs are sensitive to hypoxic stress in PEGylated fibrin gels. Despite limited cell proliferation, hypoxia did not significantly hinder the ability of these cells to form tubular networks and encouraged further production of secreted proteins important in neovascularization.

Fibrin bioactivity induces baseline endothelial marker expression

After examining the morphological and functional consequences of hypoxia in PEGylated fibrin matrices, we sought to refine the specific roles of hypoxia and matrix cues on the expression of endothelial markers in MSC networks. This aim was subdivided into two experiments: a 2D study under normoxia to establish baseline behavior and a 3D study under both normoxia and hypoxia to ascertain any gain-of-function changes.

In the first experiment, MSCs were cultured as a two-dimensional monolayer on top of a thin gel (either 4mg/mL fibrin, 4F, or 4mg/mL PEGylated fibrin, 4P), eliminating gel-

associated diffusion gradients (Sahai et al., 2012). Collagen was added as a third experimental group to control for fibrin content (4mg/mL collagen, 4C). Western blot was performed in triplicate (Figure 5F) and the chemiluminescent signal normalized to β-actin for vWF and VE-cadherin proteins. Statistical analysis revealed that MSCs on PEGylated fibrin (4P) and fibrin gels (4F) expressed similar quantities of both endothelial markers in 2D (Figure 5G & H). MSCs on collagen (4C), however, had significantly diminished endothelial protein expression compared to MSCs on PEGylated fibrin. These results imply that (1) PEGylation does not interfere with the bioactivity of fibrin proteins and (2) fibrin alone is responsible for a basal level of endothelial-like MSC character.

PEGylation-associated hypoxic stress synergistically enhances fibrin cues

In the second experiment, typical 3D culture of MSCs in PEGylated fibrin (10P) and fibrin (10F) were compared for endothelial marker expression under normoxia (Figure 5A & B, I–K). Western blot for vWF and VE-cadherin showed that PEGylated fibrin encourages significantly greater expression of both markers over unmodified fibrin alone (Figure 5J & K). Since the 2D study indicated that fibrin content encourages similar basal levels of vWF and VE-cadherin regardless of PEGylation, the new difference observed in 3D culture can be attributed to PEGylation-associated changes to the matrix environment. When both 3D matrices were cultured under 1% O_2, MSC expression of vWF and VE-cadherin was once again similar (Figure 5C & D, L–N). We hypothesize the re-equilibration of MSC endothelial character under 1% O_2 is reflective of fibrin-encapsulated MSCs gaining function (Majumdar et al., 2013; Razban et al., 2012), PEGylated fibrin-encapsulated MSCs experiencing diminished benefits from applied hypoxia, or a combination of both.

Morphological quantification was again applied to compare networks lengths. Again, under normoxia and hypoxia, cells in fibrin (10F) remained significantly shorter than cells in PEGylated fibrin (10P, Figure 5E). However, even with hypoxic stress and increased endothelial marker expression, MSCs in fibrin networks were still unable to form substantial networks. Additionally, both hypoxic groups were statistically similar to their normoxic controls. While this result is consistent with the study shown in Figure 4, we would ordinarily expect an increase in endothelial marker expression and angiogenic proteins with an increase in network length (Kumar et al., 2011; Simionescu et al., 2012). This suggests that there is an additional feature of PEGylated fibrin that leads to extensive network formation that may be independent of the endothelial-like protein expression of MSCs.

DISCUSSION

The studies presented here sought to (1) characterize the extent of endothelial-like character in MSC tubulogenesis and (2) understand how the PEGylated fibrin matrix influences these cellular outcomes. Material characterization showed that PEGylated fibrin is associated with increased amorphous over fibrous gel character and restricted diffusion, which previous studies have linked with increased MSC tubulogenesis. Current studies find that, like normal endothelium, MSC networks in PEGylated fibrin are also hollow, upregulate VEGF and MMP-2 production, and express vWF and VE-cadherin. Our studies have identified that fibrin is responsible for a basal endothelial profile while hypoxia serves to enhance

differentiation of MSCs further towards an endothelial phenotype. Robust vascular morphology, on the other hand, was most significantly associated with fibrin PEGylation rather than the biochemical nature of the matrix or the oxygen tension in culture. These results suggest that morphology depends upon a physical matrix quality apart from typical biochemical cues. We hypothesize that guidance tunnels, previously identified in normal neovascular sprouts, are able to remain patent in semi-amorphous PEGylated fibrin and have a tendency to collapse in fibrin. Unmodified fibrin exhibits a higher loss tangent at the same concentration, leading to a greater degree of viscous flow for the same value of storage modulus. This theory is supported by the time-lapse video of MSC tubulogenesis (Supplemental Figure 2) where we observe some cells retracing tunneled paths.

The lack of PECAM-1 expression, however, led us to question the extent of MSC differentiation towards an endothelial cell type (Pusztaszeri et al., 2006). An adjunct study (Supplemental Figure 3) demonstrated clear differences between MSCs and endothelial cells in their ability to form networks and express endothelial markers. While endothelial cells more strongly express vascular markers such as VE-cadherin and vWF, MSCs are more capable of migrating through matrices and establishing networks, a feature more typical of stromal than endothelial populations (Ghajar et al., 2010). Endothelial cells have a well-documented need for a supporting stromal population to fully form extended and stable networks; co-cultures are typically employed to rescue their lack of endogenously produced MMPs. Fibroblasts and MSCs have each been used as pericyte support cells in such cases (Athanassopoulos et al., 2012; Ghajar et al., 2010; Lesman et al., 2011; Oberringer et al., 2007). Interestingly, fibroblasts (used as a negative control in this adjunct study) were also able to match the ability of MSCs to form networks and express vascular markers, suggesting two possibilities: that fibroblasts posses a greater degree of phenotypic plasticity than previously anticipated (Alt et al., 2011; Blasi et al., 2011) or that a MSC networks retain fibroblastic features of their undifferentiated state alongside newly acquired endothelial behaviors. To our knowledge, only one report has previously described the ability of fibroblasts to adopt endothelial character; their *in vitro* methodology employed traditional monolayer culture supplemented by growth factors (Karlsson et al., 2009).

In literature, another neovascularization process has been similarly described in which cells are similarly characterized as VE-cadherin (+) but PECAM-1 (−) and highly dependent on MMP-2 production: vasculogenic mimicry (Folberg and Maniotis, 2004; Hendrix et al., 2001; Hess et al., 2003). Vasculogenic mimicry is a unique process whereby dense tumors overcome hypoxic stress by creating tumor-lined pseudovasculature. Described by Maniotis *et al* in 1999, vasculogenic mimicry was the first evidence demonstrating that non-endothelialized microvessels are capable of transporting blood without clotting (Maniotis et al., 1999). In terms of tissue engineering strategies, vasculogenic mimicry represents a neovascularization process where a single stromal-type population is driven (primarily) by matrix cues and hypoxic stress towards endothelial-like structure and function (Vartanian, 2012; Zhao et al., 2012). Although these non-endothelialized networks are more leaky and less efficient than normal vasculature, they are functional *enough* to facilitate blood transport and tumor survival.

While we did not look at an exhaustive profile of endothelial markers (vWF, VE-cadherin, PECAM-1, VEGF and MMP-2 in this study), the parallels between MSC tubulogenesis and vasculogenic mimicry provide a novel perspective towards understanding lesser-described stromal cell states. In cancer, these hybrid cell states are well documented. In fact, the classical epithelial-to-mesenchymal transition is often classified as "partial," where epithelial cells exhibit increased migration without complete loss of cell-cell adhesion and polarity (Kalluri and Weinberg, 2009). Here, we describe adult stem cells exhibiting increased endothelial characteristics while retaining some of their original fibroblastic traits. We propose that transitional phenotypes in stem cell biology may similarly be a third state with functional utility and worthy of further investigation.

In regards to therapeutic neovascularization, endothelial-*like* networks may provide a clinically feasible pseudovasculature for temporarily sustaining grafts until the host vasculature is able to infiltrate and remodel tissue. The ability of fibroblasts to match endothelial-*like* MSC behavior suggests that this mechanism of tubulogenesis may be shared amongst other cells of stromal lineage. Tubulogenesis is a major mechanism of normal embryological development and organogenesis as well as a potent mechanism of metastatic invasion (Lubarsky and Krasnow, 2003; Nagle and Cress, 2011). However, *stromal* tubulogenesis in non-diseased adult biology lacks documentation; further studies would be necessary to determine whether this cell behavior is an artifact of *in vitro* culture or simply a rare natural phenomenon. If tubulogenesis is in fact a latent but inducible stromal function, the work here has the potential to open up new cell sources as therapeutically valuable for neovascularization strategies.

Supplementary Material

Refer to Web version on PubMed Central for supplementary material.

ACKNOWLEDGMENTS

Abbreviations

MCBs	microcarrier beads
MMP	matrix metalloproteinase
MSCs	mesenchymal stem cells
PECAM-1	platelet endothelial cell adhesion molecule
PEG	polyethylene glycol
VE-cadherin	vascular endothelial cadherin

VEGF   vascular endothelial growth factor

vWF   von Willebrand factor

REFERENCES

Alt E, Yan Y, Gehmert S, Song Y-H, Altman A, Gehmert S, Vykoukal D, Bai X. Fibroblasts share mesenchymal phenotypes with stem cells, but lack their differentiation and colony-forming potential. Biol Cell. 2011; 103:197–208. [PubMed: 21332447]

Athanassopoulos A, Tsaknakis G, Newey SE, Harris AL, Kean J, Tyler MP, Watt SM. Microvessel networks in pre-formed in artificial clinical grade dermal substitutes in vitro using cells from haematopoietic tissues. Burns. 2012; 38:691–701. [PubMed: 22360956]

Bayless K, Davis G. The Cdc42 and Rac1 GTPases are required for capillary lumen formation in three-dimensional extracellular matrices. J Cell Sci. 2002; 115:1123–1136. [PubMed: 11884513]

Blasi A, Martino C, Balducci L, Saldarelli M, Soleti A, Navone SE, Canzi L, Cristini S, Invernici G, Parati EA, Alessandri G. Dermal fibroblasts display similar phenotypic and differentiation capacity to fat-derived mesenchymal stem cells, but differ in anti-inflammatory and angiogenic potential. Vasc Cell. 2011; 3:5. [PubMed: 21349162]

Davis GE, Bayless KJ, Mavila A. Molecular basis of endothelial cell morphogenesis in three-dimensional extracellular matrices. Anat. Rec. 2002; 268:252–275. [PubMed: 12382323]

Davis GE, Camarillo CW. An alpha 2 beta 1 integrin-dependent pinocytic mechanism involving intracellular vacuole formation and coalescence regulates capillary lumen and tube formation in three-dimensional collagen matrix. Experimental Cell Research. 1996; 224:39–51. [PubMed: 8612690]

Fadini GP, Agostini C, Avogaro A. Autologous stem cell therapy for peripheral arterial disease meta-analysis and systematic review of the literature. Atherosclerosis. 2010; 209:10–17. [PubMed: 19740466]

Falanga V, Iwamoto S, Chartier M, Yufit T, Butmarc J, Kouttab N, Shrayer D, Carson P. Autologous bone marrow-derived cultured mesenchymal stem cells delivered in a fibrin spray accelerate healing in murine and human cutaneous wounds. Tissue Eng. 2007; 13:1299–1312. [PubMed: 17518741]

Folberg R, Maniotis AJ. Vasculogenic mimicry. APMIS. 2004; 112:508–525. [PubMed: 15563313]

Galas RJ, Liu JC. Vascular endothelial growth factor does not accelerate endothelial differentiation of human mesenchymal stem cells. J. Cell. Physiol. 2013

Ghajar CM, Kachgal S, Kniazeva E, Mori H, Costes SV, George SC, Putnam AJ. Mesenchymal cells stimulate capillary morphogenesis via distinct proteolytic mechanisms. Experimental Cell Research. 2010; 316:813–825. [PubMed: 20067788]

Gibot L, Galbraith T, Huot J, Auger FA. A preexisting microvascular network benefits in vivo revascularization of a microvascularized tissue-engineered skin substitute. Tissue Engineering Part A. 2010; 16:3199–3206. [PubMed: 20528673]

Hendrix MJ, Seftor EA, Meltzer PS, Gardner LM, Hess AR, Kirschmann DA, Schatteman GC, Seftor RE. Expression and functional significance of VE-cadherin in aggressive human melanoma cells: role in vasculogenic mimicry. Proc Natl Acad Sci USA. 2001; 98:8018–8023. [PubMed: 11416160]

Hess AR, Seftor EA, Seftor REB, Hendrix MJC. Phosphoinositide 3-kinase regulates membrane Type 1-matrix metalloproteinase (MMP) and MMP-2 activity during melanoma cell vasculogenic mimicry. Cancer Res. 2003; 63:4757–4762. [PubMed: 12941789]

Kalluri R, Weinberg RA. The basics of epithelial-mesenchymal transition. J. Clin. Invest. 2009; 119:1420–1428. [PubMed: 19487818]

Karlsson LK, Junker JPE, Grenegard M, Kratz G. Human Dermal Fibroblasts: A Potential Cell Source for Endothelialization of Vascular Grafts. Ann Vasc Surg. 2009; 23:663–674. [PubMed: 19576728]

Kim CH, Lee JH, Won JH, Cho MK. Mesenchymal stem cells improve wound healing in vivo via early activation of matrix metalloproteinase-9 and vascular endothelial growth factor. J. Korean Med. Sci. 2011; 26:726–733. [PubMed: 21655056]

Kumar G, Tison CK, Chatterjee K, Pine PS, McDaniel JH, Salit ML, Young MF, Simon CG. The determination of stem cell fate by 3D scaffold structures through the control of cell shape. Biomaterials. 2011; 32:9188–9196. [PubMed: 21890197]

Lesman A, Koffler J, Atlas R, Blinder YJ, Kam Z, Levenberg S. Engineering vessel-like networks within multicellular fibrin-based constructs. Biomaterials. 2011; 32:7856–7869. [PubMed: 21816465]

Lubarsky B, Krasnow MA. Tube morphogenesis: making and shaping biological tubes. Cell. 2003

Lutolf MP, Gilbert PM, Blau HM. Designing materials to direct stem-cell fate. Nature. 2009; 462:433–441. [PubMed: 19940913]

Majumdar D, Bhonde R, Datta I. Influence of ischemic microenvironment on human Wharton's Jelly mesenchymal stromal cells. Placenta. 2013

Maniotis AJ, Folberg R, Hess A, Seftor EA, Gardner LM, Pe'er J, Trent JM, Meltzer PS, Hendrix MJ. Vascular channel formation by human melanoma cells in vivo and in vitro: vasculogenic mimicry. Am. J. Pathol. 1999; 155:739–752. [PubMed: 10487832]

Nagle RB, Cress AE. Metastasis Update: Human Prostate Carcinoma Invasion via Tubulogenesis. Prostate Cancer. 2011; 2011:249–290.

Nakatsu MN, Davis J, Hughes CCW. Optimized Fibrin Gel Bead Assay for the Study of Angiogenesis. J Vis Exp. 2007

Nakatsu MN, Hughes CCW. An optimized three-dimensional in vitro model for the analysis of angiogenesis. Meth. Enzymol. 2008; 443:65–82. [PubMed: 18772011]

Nehls V, Drenckhahn D. A novel, microcarrier-based in vitro assay for rapid and reliable quantification of three-dimensional cell migration and angiogenesis. Microvasc Res. 1995; 50:311–322. [PubMed: 8583947]

Oberringer M, Meins C, Bubel M, Pohlemann T. A new in vitro wound model based on the co-culture of human dermal microvascular endothelial cells and human dermal fibroblasts. Biol Cell. 2007; 99:197–207. [PubMed: 17222082]

Piret J-P, Mottet D, Raes M, Michiels C. CoCl2, a chemical inducer of hypoxia-inducible factor-1, and hypoxia reduce apoptotic cell death in hepatoma cell line HepG2. Ann N Y Acad Sci. 2002; 973:443–447. [PubMed: 12485908]

Pusztaszeri MP, Seelentag W, Bosman FT. Immunohistochemical expression of endothelial markers CD31, CD34, von Willebrand factor, and Fli-1 in normal human tissues. Journal of Histochemistry and Cytochemistry. 2006; 54:385–395. [PubMed: 16234507]

Razban V, Lotfi AS, Soleimani M, Ahmadi H, Massumi M, Khajeh S, Ghaedi M, Arjmand S, Najavand S, Khoshdel A. HIF-1α Overexpression Induces Angiogenesis in Mesenchymal Stem Cells. Biores Open Access. 2012; 1:174–183. [PubMed: 23514846]

Rytlewski JA, Geuss LR, Anyaeji CI, Lewis EW, Suggs LJ. Three-dimensional image quantification as a new morphometry method for tissue engineering. Tissue Engineering Part C: Methods. 2012; 18:507–516. [PubMed: 22224751]

Sahai S, McFarland R, Skiles ML, Sullivan D, Williams A, Blanchette JO. Tracking hypoxic signaling in encapsulated stem cells. Tissue Engineering Part C: Methods. 2012; 18:557–565. [PubMed: 22250882]

Shamloo A, Heilshorn SC. Matrix density mediates polarization and lumen formation of endothelial sprouts in VEGF gradients. Lab Chip. 2010; 10:3061–3068. [PubMed: 20820484]

Simionescu DT, Chen J, Jaeggli M, Wang B, Liao J. Form Follows Function: Advances in Trilayered Structure Replication for Aortic Heart Valve Tissue Engineering. J Healthc Eng. 2012; 3:179–202. [PubMed: 23355946]

Vartanian AA. Signaling pathways in tumor vasculogenic mimicry. Biochemistry Mosc. 2012; 77:1044–1055. [PubMed: 23157265]

Zhang G, Drinnan CT, Geuss LR. Vascular differentiation of bone marrow stem cells is directed by a tunable three-dimensional matrix. Acta Biomater. 2010; 6:3395–3403. (null). [PubMed: 20302976]

Zhao N, Sun B-C, Sun T, Ma Y-M, Zhao X-L, Liu Z-Y, Dong X-Y, Che N, Mo J, Gu Q. Hypoxia-induced vasculogenic mimicry formation via VE-cadherin regulation by Bcl-2. Med Oncol. 2012; 29:3599–3607. [PubMed: 22562824]

Highlights

- We examine mechanisms of spontaneous MSC tubulogenesis in PEGylated fibrin gels

- Fibrin provides angiogenic bioactivity and PEGylation induces mild hypoxia

- Hypoxia enhances the endothelial phenotype of MSCs but not network formation

- These networks lack full endothelial maturity (VEcadherin+/PECAM1−)

- MSCs exhibit both endothelial and stromal features, similar to vasculogenic mimicry
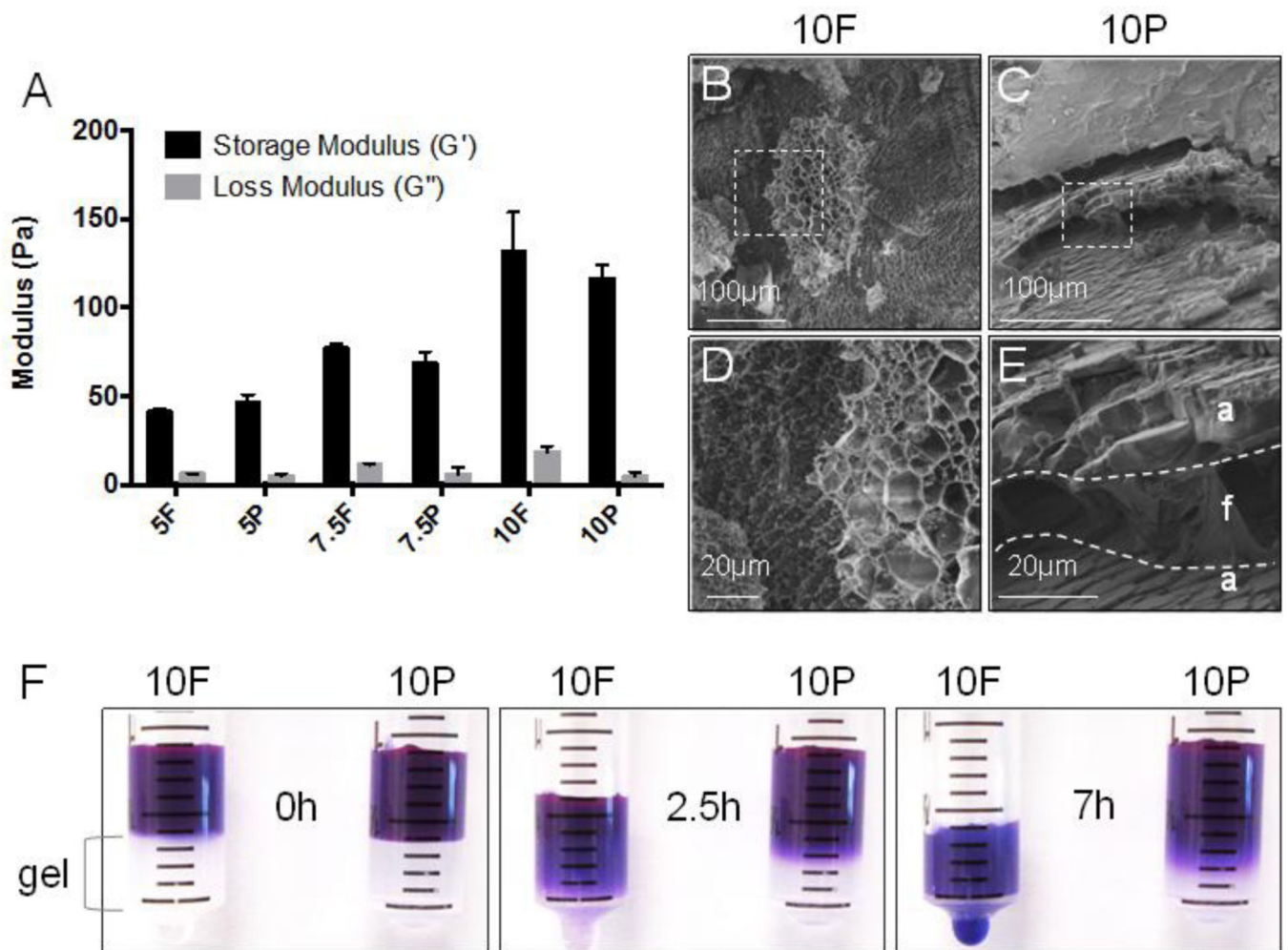
Fig. 1.
Characterization of fibrin and PEGylated fibrin gel properties. Abbreviations: F, unmodified fibrin; P, PEGylated fibrin; 5, 7.5, 10 indicate mg/mL of fibrin. (A) Rheological analysis of storage and loss moduli for fibrin and PEGylated fibrin across three increasing fibrin concentrations. (B–E) Cryo SEM of fractured gel cross-sections at 10mg/mL fibrin content. Images (D) and (E) are magnified views of the insets from (B) and (C), respectively. (F) Time-lapse photography: diffusion of 10kDa dextran-Texas Red through fibrin and PEGylated fibrin gels within syringe mold. *p < 0.05, versus fibrin control
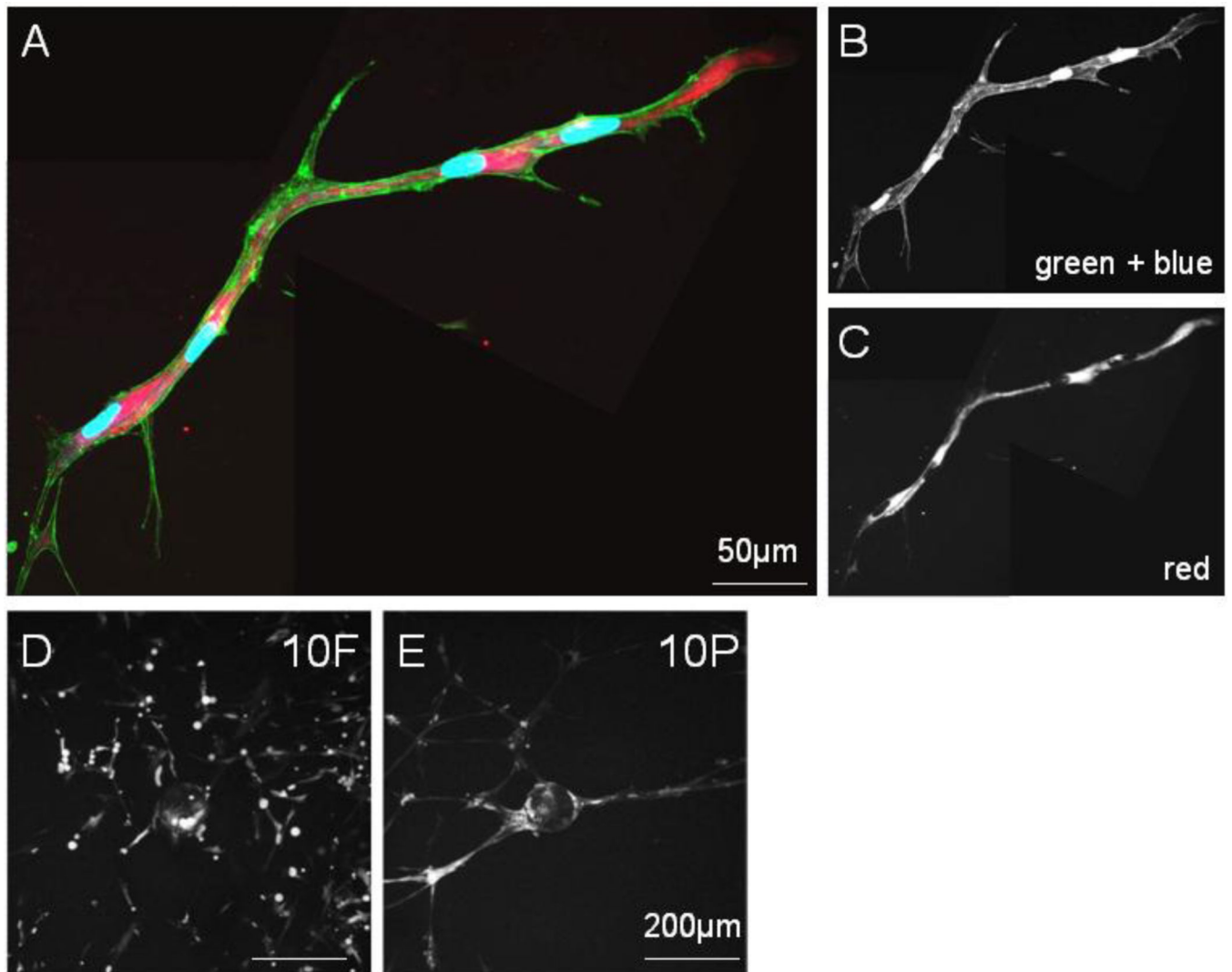
Fig. 2.
Lumen development of MSC networks in PEGylated fibrin. Two stitched frames of a single tubular structure. (A) Merged fluorescent channels from (B) and (C); (B) FITC-phalloidin labeling of f-actin filaments with DAPI staining of nuclei and (C) dextran-Texas Red localization in vesicles, scale bar = 50μm
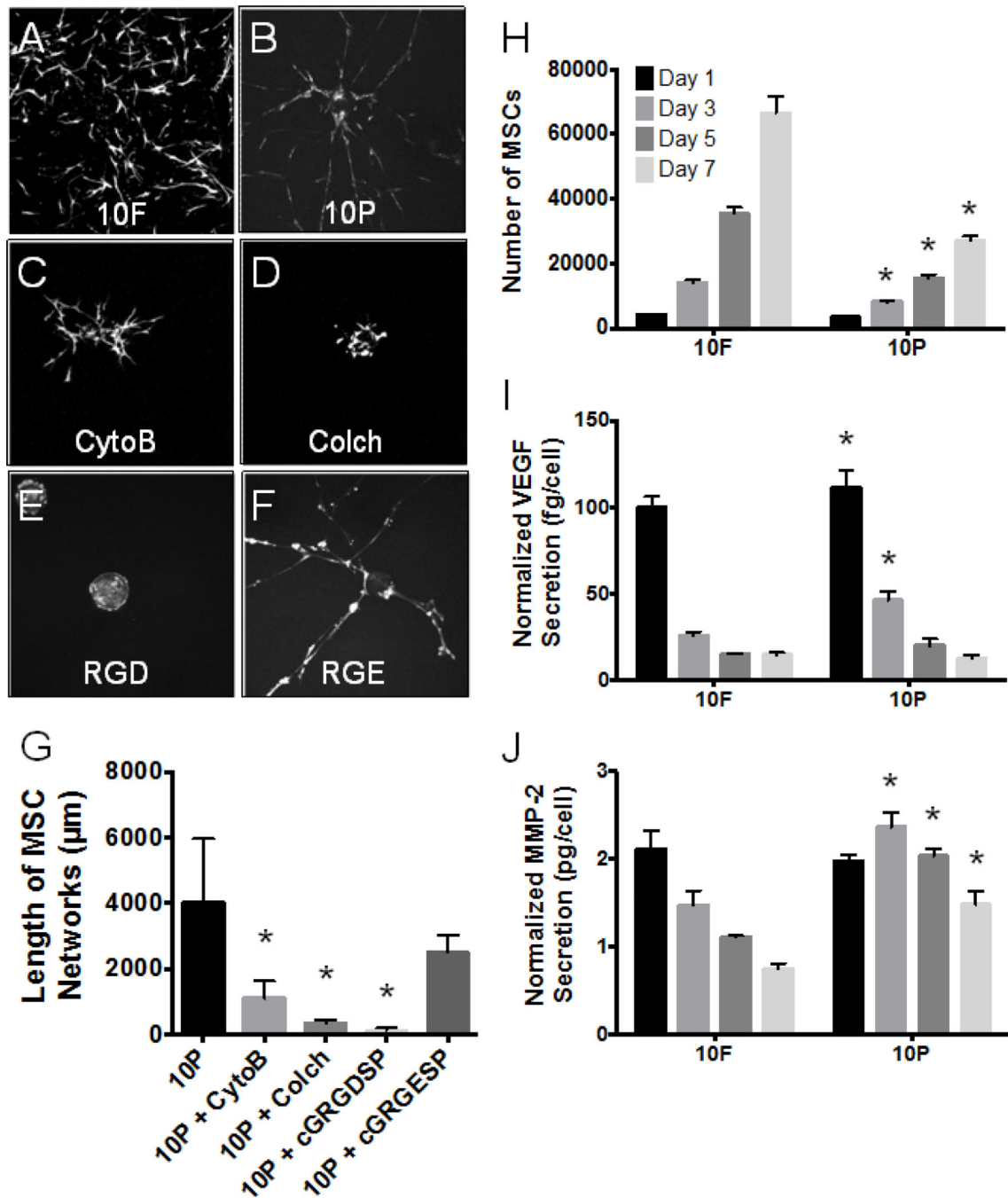
Fig. 3.
Characterization of MSC behavior. Abbreviations: CytoB, cytochalasin B; Colch, colchicine; RGD, cyclic-GRGDSP; RGE, cyclic-GRGESP; 10F, 10mg/mL unmodified fibrin; 10P, 10mg/mL PEGylated fibrin. (A–F) Fluorescent z-stack projections using standard deviation pixel intensities; images are representative of each group. (G) Average network length per microcarrier bead as measured by our 3D quantification method. (H) Results of the Celltiter 96 assay. (I) VEGF secretion and (J) MMP-2 secretion normalized to

cell number from (H). (G) *p < 0.05, versus 10P control; (H–J) *p < 0.05, versus 10F control at same time point
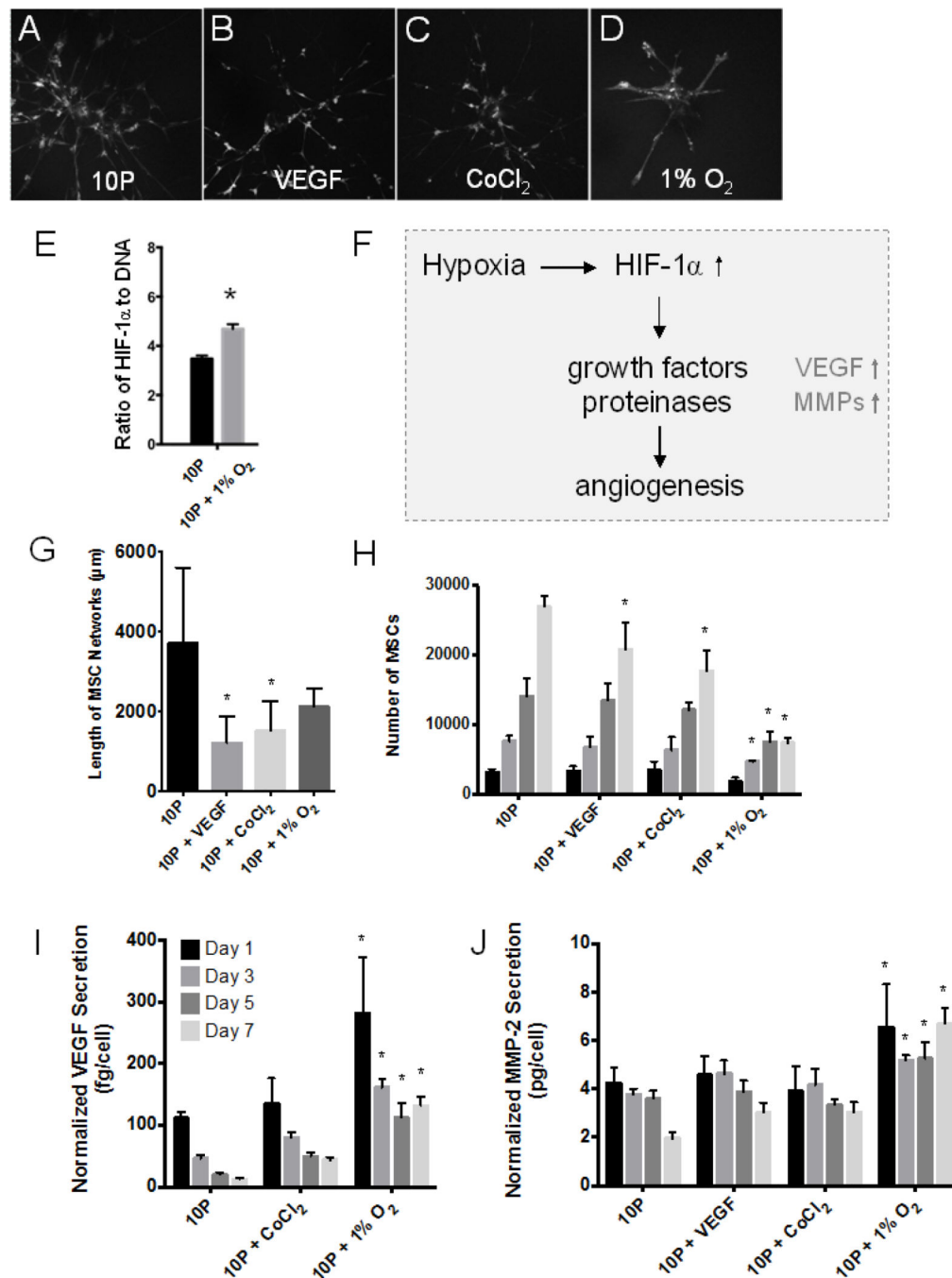
Fig. 4.
VEGF and hypoxia stimuli study. Abbreviations: 10P, 10mg/mL PEGylated fibrin. (A–D)
Fluorescent z-stack projections representative of morphological outcomes in (G). (E)
HIF-1α production quantified by ELISA and normalized to total DNA content by nanodrop.
(F) General mechanism of hypoxia-induced neovascularization, linking hypoxia with
increased VEGF and MMP-2 production. (G) Average network lengths per microcarrier
bead as measured by our 3D quantification method. (H) Results of Celltiter 96 assay
indicated no mitogenic response to VEGF or CoCl2 but a significant decline in MSC

proliferation under 1% O_2. Hypoxic stress increased VEGF secretion (I) and MMP-2 production (J) of MSCs in PEGylated fibrin; values are normalized to cell numbers reported in (F). $*p < 0.05$, versus 10P control at same time point
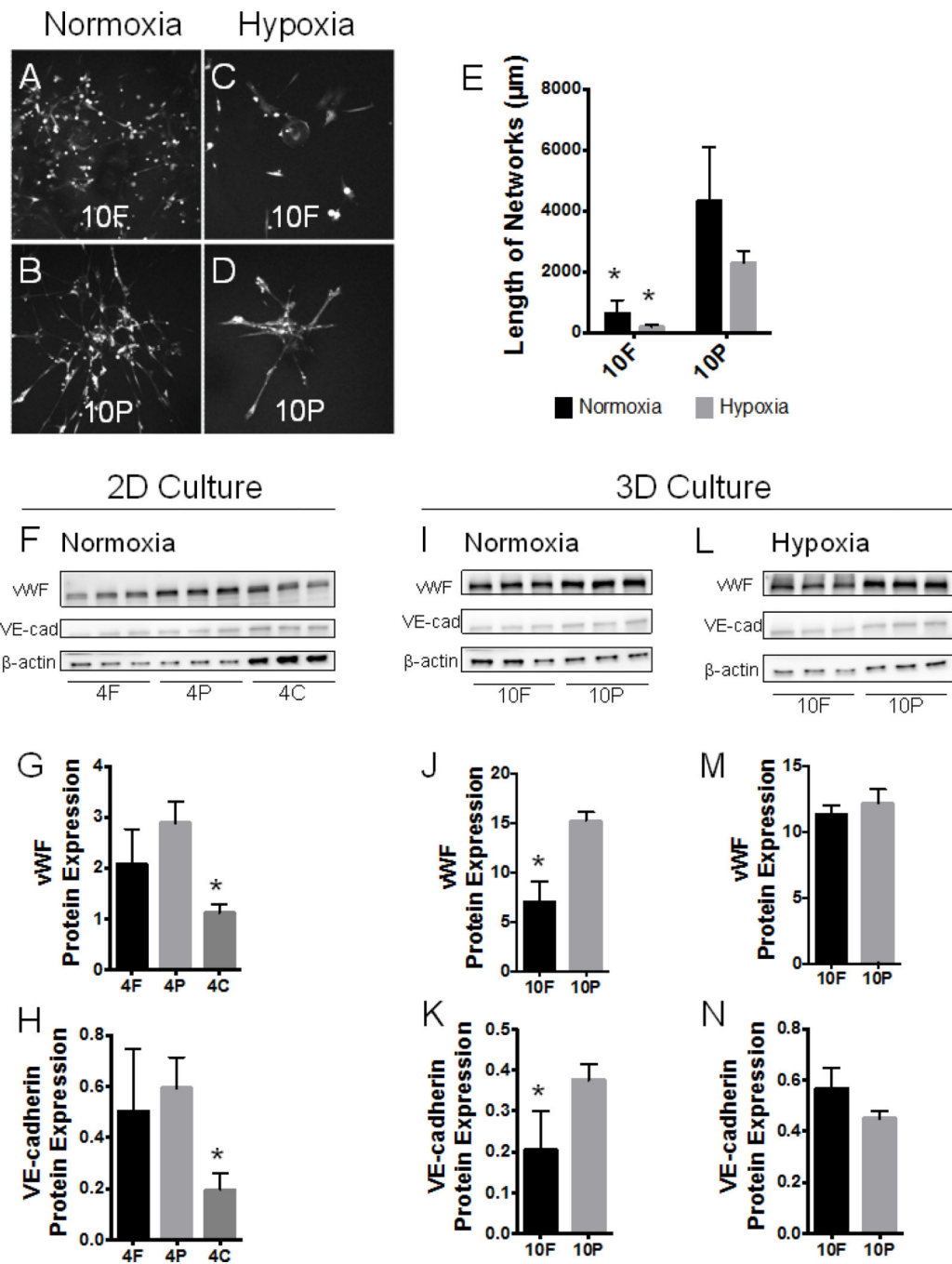
Fig. 5.
Substrate cues versus hypoxic stress. Abbreviations: 10F, 10mg/mL umodified fibrin; 10P, 10mg/mL PEGylated fibrin. (A–D) Fluorescent z-stack projections representative of MSCs in PEGylated fibrin and fibrin under normoxic and hypoxic culture. (E) 3D morphological quantification of network length for groups shown in (A–D). (F–H) MSCs were seeded on top of thin gel substrates and cultured for 7 days under normoxic conditions. Chemiluminescent signal from Western blots (shown in F) of vWF and VE-cadherin protein were normalized to sample-appropriate β-actin signal in G and H, respectively. (I–N)

Comparison of normoxia- and hypoxia-induced endothelial marker expression in 3D gel culture of MSCs. MSCs were seeded on microcarrier beads and encapsulated within gels, as previously described. Under normoxic conditions, chemiluminescent signal (shown in I) of vWF and VE-cadherin protein were normalized to sample-appropriate β-actin signal in J and K, respectively. Under 1% O_2 hypoxic conditions, chemiluminescent signal (shown in L) of vWF and VE-cadherin protein were normalized to sampleappropriate β-actin signal in M and N, respectively. *$p < 0.05$, versus PEGylated fibrin in (G, H, J, K, M, N), versus normoxic control in (E)

Table 1

Exogenous peptides and small molecules used in experimental groups.

Molecule	Concentration	Study	Manufacturer
Cyclo-GRGDSP	500 μg/mL	MIC-axis	AnaSpec
Cyclo-GRGESP	500 μg/mL	MIC-axis	AnaSpec
Cytochalasin B	0.1 μM	MIC-axis	Sigma-Aldrich
Colchicine	0.1 μM	MIC-axis	Sigma-Aldrich
Human VEGF-165	50 ng/mL	HIF-axis	BioLegend
Cobalt chloride	75μM	HIF-axis	Fisher Scientific

Table 2

Antibodies used for western blot protein detection.

Antibody target	1°/2°	Species	Dilution	Manufacturer
CD31 (clone P2B1)	primary	mouse	1:100	Abcam (ab24590)
von Willebrand factor	primary	rabbit	1:1000	Abcam (ab6994)
VE-cadherin	primary	rabbit	1:700	Abcam (ab33168)
β-actin	primary	rabbit	1:1000	Abcam (ab75186)
Mouse IgG	secondary	rabbit	1:5000	Abcam (ab6728)
Rabbit IgG	secondary	goat	1:5000	Santa Cruz Bio (sc-2004)